Calculations of adsorption and diffusion of H-atom on FCC(100) and BCC(100) transition metal surfaces

Avan Anwar Faraj

Faculty of Science
University of Iceland
2015

Calculations of adsorption and diffusion of H-atom on FCC(100) and BCC(100) transition metal surfaces

Avan Anwar Faraj

120 ECTS thesis submitted in partial fulfillment of a
Magister Scientiarum degree in Chemistry

Supervisor
Professor Hannes Jónsson

Co-advisors
Dr. Egill Skúlason
Dr. Anna Garden

Faculty of Science
School of Engineering and Natural Sciences
University of Iceland
Reykjavik, June 2015

I

Calculations of adsorption and diffusion of H-atom on FCC(100) and BCC(100) transition metal surfaces

120 ECTS thesis submitted in partial fulfillment of a *Magister Scientiarum* degree in Chemistry

Abstract

The interaction between hydrogen and a transition metal surface is an important aspect of many chemical processes, in particular heterogeneous transition metal catalysts. Density functional theory calculations are used here to study the interaction of a hydrogen adatom with open facets of 14 transition metals, either FCC(100) or BCC(100) surfaces. Potential energy surfaces are generated representing the variation of the binding energy of atomic hydrogen over the surface unit cell. On Ag, Au and Cu the adsorption of hydrogen is endothermic with respect to gas phase H_2 but on the rest of the metals it is exothermic. The activation energy for hydrogen diffusion over the surface is extracted from the calculated results. A wide variation in activation energy is found, from 0.02 eV for Pd(100) to 0.36 eV for W(100). The effect of metal atom relaxation was assessed by comparison with calculations using frozen surfaces.

Útdráttur

Víxlverkun vetnis og hliðarmálma er mikilvæg í mörgum efnaferlum, sérstaklega í misleitri efnahvötun. Þéttnifellareikningar (DFT) eru notaðir hér til að meta víxlverkun vetnisatóms á yfirborði við opin yfirborð 14 hliðarmálma, annað hvort FCC(100) eða BCC(100) yfirborð. Niðurstöðurnar gefa orkuyfirborð sem sýnir hvernig bindiorka atómsins breytist yfir einingarsellu yfirborðanna. Á Ag, Au og Cu er ásog vetnisins innvermið með tilliti til H_2 í gasfasa en útvermið á hinum yfirborðunum. Virkjunarorka fyrir sveim vetnisins á yfirborðunum er einnig reiknuð út. Virkjunarorkan er mjög mismunandi eftir yfirborðum, frá 0.02 eV á Pd(100) og upp í 0.36 eV á W(100). Áhrif á færslu atómanna er meting með samanburði við frosin yfirborð.

To my children

Lenya Rún

Lawand Ari

Lano Ares

Table of Contents

List of Figures

List of Tables

List of Abbreviations

DFT	Density functional theory
PES	Potential energy surface
MEP	Minimum energy path
Relaxed system	The slab with tow bottom layers and one surface atom fixed
Fixed system	The slab with tow bottom layers and the surface layer fixed

x

Acknowledgements

Chapter 1

Introduction

Heterogeneous catalysis is extremely important for the chemical industry as well as many other aspects of modern life. An improvement in its efficiency can help reduce cost of energy and products and the possibility now exists to use computational calculations to help design new and better catalysts. A large amount of fundamental research is being done by industrial companies and university research laboratories to determine how catalysts work and to improve their effectiveness. If the catalytic activity of a given process can be improved, it may be possible to lower the temperature and/or pressure required and in this way large amount of energy could be saved. Furthermore, it may be possible to reduce the amount of reactants that are wasted forming unwanted by-products.

A heterogeneous catalyst is in a different phase than the reactants and products. Such catalysts are often favored in industry since they can easily be separated from the products, although they are often less specific than homogeneous catalysts in that more side reactions can occur.

The interaction between gaseous or solvated hydrogen with a transition metal surface plays an important role in many chemical processes. Hydrogenolysis, hydrogenation and dehydrogenation are all important in many chemical industries [1] [2], and most of these reactions take place on heterogeneous transition metal catalysts [3] [4]. An essential step towards understanding these reactions is the elucidation of the interaction of hydrogen with the catalyst surface. Computer calculations combined with the development of models and theories of catalysis have become an important approach for understanding and improving the design of heterogeneous catalysts.

In the present study, the interaction of a hydrogen atom with the surface of several, open transition metal surfaces (the (100) facets of body-centered cubic (BCC) metals and face-

centered cubic (FCC) metals) is investigated using density functional theory (DFT) [5]. The binding energy as well as activation energy for the diffusion of hydrogen over the surfaces is determined. The effect of the magnetic state of Ni and Fe on the adsorption geometry and diffusion of hydrogen has also been addressed. The calculations were carried out for a total of 14 transition metals, BCC(100) surfaces of V, Fe, Nb, Mo, Ta and W, and FCC(100) surfaces of Ni, Cu, Rh, Pd, Pt, Ag, Au and Ir.

This work adds to and complements an earlier study of hydrogen interaction with the close packed surfaces of several metals, FCC(111) and BCC(110). [6]

Chapter 2

Theory

2.1 Density Functional Theory

Density functional theory (DFT) is a highly successful and widely used quantum mechanical method for approximating the solution of the Schrödinger equation for a system of electrons. It can be used to estimate the ground state of large, many-electron systems, such as atoms, molecules and materials. DFT is, in principle, an *ab initio* method, meaning that it does not make use of any fitting to experimental results on chemical bonding. It works with the electron density as the basic quantity. Whereas the wave function of a system containing N electrons is dependent on 3N variables (three spatial variables for each of the N electrons), the density is only a function of three spatial variables and therefore is a simpler quantity to deal with.

The extent to which DFT has contributed to the chemical, physical and biological sciences is reflected by the 1998 Nobel prize in chemistry, which was awarded to Walter Kohn [5] for the development of DFT, along with John Pople [7] for the development of quantum chemistry.

2.1.1 The Schrödinger Equation

The electronic Schrödinger equation can be used for non-relativistic description of a system of N electrons

$$\widehat{H}\psi = E\psi \qquad (2.1)$$

E is the total energy, $\psi = \psi(r_1, r_2, r_3,,\ldots,r_N)$ is the wave function depending on the spatial coordinates, r_i, of each electron, and $\widehat{H}$ is the Hamiltonian operator. The Hamiltonian may be decomposed into the relative kinetic and potential contributions as:

$$\hat{H} = \hat{K} + \hat{U} + \hat{v} \tag{2.2}$$

where

$$\hat{K} = \sum_i -\frac{1}{2}\nabla_i^2 \tag{2.3}$$

$$\hat{U} = \sum_i \sum_{j>i} \frac{1}{r_{ij}} \tag{2.4}$$

and

$$\hat{v} = \sum_i \sum_A \frac{1}{r_{iA}} + V_{ext} \tag{2.5}$$

$\hat{K}$ is the kinetic energy operator, $\hat{U}$ is the interaction between electron pairs and $\hat{v}$ is the interaction between electrons and the external potential (representing interaction with the nuclei). In equation 2.4, r_{ij} is the distance between electron j and electron i and in equation 2.5 the $\frac{1}{r_{iA}}$ term is the distance between electron i and nucleus A, while V_{ext} is the external potential.

2.1.2   The Hohenberg-Kohn Theorem

The foundation of the DFT method is the Hohenberg-Kohn theorem, which states that for each given electronic density ρ(r) there is one and only one corresponding potential. Once this has

been established, it can be seen that the total energy is a unique functional of the electron density, $\rho(r)$, which is an observable while the wave function is not.

$$E[\rho(r)] = \langle \psi[r] | \hat{H} | \psi[r] \rangle \qquad (2.6)$$

The Raleigh-Ritz variational principle is used to minimize the energy and find the ground state energy and density,

$$E_0 = \min_{\rho(r)}(E[\rho(r)]) \qquad (2.7)$$

This is the basis of modern day DFT.

2.1.3   The Kohn-Sham Equation

While the Hohenberg-Kohn theorem provides a foundation for DFT, it does not say anything about the form of the functional. Kohn and Sham [8] proposed in 1965 an approach for approximating the functional by mapping the interacting many-electron system onto a system of non-interacting electrons described by orbitals, $\{\Phi_i\}$, where each electron is subject to the average interaction with of all other electrons. The orbitals are one-electron wave functions that can be found by solving the Kohn-Sham equations

$$\left\{ -\frac{1}{2} \nabla^2 + v_{eff} r(r) \right\} \phi_i(r) = \epsilon_i \phi_i(r) \qquad (2.8)$$

Since both the effective potential and the wave functions are unknown, these equations must be solved self-consistently. The electron density can then be produced using the magnitude squared of the wave functions:

$$\rho(r) = \sum_{i=1}^{N} |\emptyset_i(r)|^2 \qquad (2.9)$$

The effective potential can be written as

$$v_{eff}(r) = v(r) + v_H(r) + v_{XC}(r) \qquad (2.10)$$

$v(r)$ is the sum of the kinetic and static potentials, $v_H(r)$ is the Hartree potential describing the electron-electron Coulumb repulsion and $v_{XC}(r)$ is the exchange-correlation potential.

$$v_H(r) = \int d^3r \, \frac{\rho(r')}{|r - r|} \qquad (2.11)$$

$$v_{XC}(r) = \frac{\delta E_{XC}[\rho]}{\delta \rho(r)} \qquad (2.12)$$

2.1.4 The Exchange-Correlation Functional

Kohn and Sham [8] proposed a local density approximation (LDA) to the exchange-correlation energy. In LDA, only the density at the coordinates where the functional is evaluated is used,

$$E_{XC}[\rho] = \int d^3r \epsilon_{XC} [\rho, r] \rho(r) \qquad (2.13)$$

The $\epsilon_{XC}(\rho, r)$ is the exchange correlation energy density. A more accurate approximation can be obtained by including also the gradient of the density, a semi-local functional. Here, the so called Generalized Gradient Approach (GGA) functional based on the Pedrew, Burke, Ernzerhof (PBE) [9] was used. GGA uses the exchange-correlation energy of a homogeneous

electron gas at point r, similar to LDA, [8] but also uses the gradient of the density to account for inhomogeneity in the electron density.

$$s(r) = \frac{|\nabla\rho(r)|}{2\sqrt[3]{3\pi^2\rho(r)}}\frac{1}{\rho(r)} \tag{2.14}$$

The GGA functional is significantly more accurate than LDA and typically gives good results, usually predicting interatomic distances in molecules with an accuracy of ±0.02 Å and energy differences within 0.1 to 0.2 eV, with some notable exceptions though (the bond in the O_2 molecule being a particularly bad, with overbinding of nearly 1 eV) [10].

For systems with unpaired electrons, the functional depends on both the spin-up and spin-down electron density. This can be introduced in a local fashion in the local spin density (LSD) approximation, or – more accurately - the spin polarized GGA approximation, which is given as:

$$E_{xc}^{GGA} = \int \epsilon_{xc}^{GGA}(\rho\uparrow,\rho\downarrow,\nabla\rho\uparrow,\nabla\rho\downarrow)\rho(r)d^3r \tag{2.15}$$

2.1.5   Plane Wave Basis Set

Two of the most commonly used basis sets are plane waves and Gaussian functions. In our calculations, which are performed using the Vienna *ab initio* simulation package [11] [12] [13] [14], the wave functions are expanded using plane waves since we apply periodic boundary conditions. Using Bloch's theorem [15], the orbitals can be written as

$$\psi_k^m(r) = \sum_{K+G} C_{K+G}^m \, e^{i(K+G)\cdot r} \tag{2.16}$$

Here G denotes the reciprocal lattice vectors, k is a vector of real numbers called the crystal wave vector. Typically, a finite number of plane-wave functions are used, below a specific cutoff energy which is chosen for each calculation. These basis sets are commonly used in

calculations involving periodic boundary conditions. The number of plane waves can be represented by defining a cutoff, G_{cut}, where the corresponding kinetic energy is less than a cutoff energy

$$\left(\frac{h^2}{2m}\right)|k + G_{cut}|^2 \leq E_{cut} \tag{2.17}$$

In order to reduce the number of plane waves needed, and thereby the energy cutoff, E_{cut}, one usually represents only the valence electrons and uses a pseudopotential to describe the interaction of the valence electrons with the core electrons and the nucleus. Pseudopotentials generally give results of good accuracy, especially so-called ultrasoft pseudopotentials with non-local components [16].

2.2 Magnetic Systems

Molecules and materials possessing a net magnetic moment are at the core of many modern technological devices, such as electrical power generators and transformers, computers, telephones and credit cards. A magnetic material is associated with a magnetic field which is at any given point specified by both a direction and a magnitude. The strength is denoted by H and the magnetic flux density denoted by B. Both B and H are field vectors, being characterized not only by magnitude, but also by direction in space. The magnetic field strength and flux density are related according to

$$B = \mu H \tag{2.18}$$

The parameter μ is called the permeability, and is a property of the specific medium through which the *H* field passes and in which *B* is measured. Another field quantity, *M*, called the magnetization of the solid, is defined by the expression

$$B = \mu_0 H + \mu_0 M \tag{2.19}$$

where μ_0 is the magnetic permeability of space. In the presence of an *H* field, the magnetic moments within a material tend to become aligned with the field and to reinforce it by virtue of their magnetic fields. The term in Equation 2.19 is a measure of this contribution.

The macroscopic magnetic properties of materials are a consequence of magnetic moments associated with individual electrons. Each electron in an atom has a magnetic moment that originates from two sources. One is related to its orbital motion around the nucleus; being a moving charge, an electron may be considered to generate a small current loop and thereby a magnetic field corresponding to a magnetic moment along its axis of rotation. Each electron also has an intrinsic magnetic moment - spin. The electron spin is a vector and can be described by its two components along an axis. Electron spin magnetic moment is typically specified by a spin "up" component and a spin "down" component. Thus each electron in an atom may be thought of as being a small magnet having orbital and permanent spin magnetic moments. The total magnetic moment of an atom is equal to the vector sum of the orbital magnetic moment and the intrinsic spin magnetic moment of all its electrons. The contribution of the nuclear magnetic moment is small and can often be neglected. Each atom with unpaired electrons acts as a magnetic dipole and produces a small, but measurable magnetic field.

Iron and nickel are well known examples of materials that exhibit magnetic properties. We will discuss their magnetic properties in Section 3.2

2.2.1   Ferromagnetic systems

Ferromagnetism arises from parallel orientation of the magnetic moments of atoms in the absence of an external field. This can lead to large and permanent magnetizations. Iron, nickel and some of the rare earths (gadolinium, dysprosium) exhibit ferromagnetic properties. Usually M is larger than H, and from equation 2.19 we can write

$$B \approx \mu_0 M \qquad (2.20)$$

The permanent magnetic moments in ferromagnetic materials result from atomic magnetic moments due to electron spin which is not cancelled out by electrons with opposite spin. The orbital magnetic moment contribution is small in comparison to the spin magnetic moment. Ferromagnetism is a so-called cooperative phenomenon, as single atoms cannot exhibit ferromagnetism, but once a number of atoms are bound together in solid form, ferromagnetic properties can arise. If a ferromagnetic material is cooled below the Curie temperature, microscopic domains with nonzero magnetization form. The Curie temperature gives an idea of the amount of energy it takes to break up the long-range magnetic ordering in the material.

2.2.2   Antiferromagnetic system

Another phenomenon of magnetism is antiferromagnetic ordering where the alignment of the electron spin moments of neighboring atoms is in exactly the opposite direction (antiparallel); the magnetism from magnetic atoms or ions oriented in one direction is canceled out by the set of magnetic atoms or ions that are aligned in the reverse direction. This spontaneous antiparallel coupling of atomic magnets is disrupted by heating and disappears entirely above a certain temperature, called the Néel temperature, characteristic of each antiferromagnetic material. (The Néel temperature is named for Louis Néel, French physicist, who in 1936 gave one of the first explanations of antiferromagnetism and was awarded the Nobel Prize in Physics for his work in 1970) [17].

2.3 Reaction Path Calculations

Finding the lowest energy path for the rearrangement of a group of atoms from one stable configuration to another is one of the important issues in theoretical chemistry and condensed matter physics. Such a paths is referred to as a minimum energy path (MEP). It is used to characterize diffusion processes in solids, changes in conformation of molecules, and chemical reactions. The MEP defines a reaction coordinate for the transition. A maximum in the energy along an MEP is a saddle point on the energy surface. It can be used to estimate the activation energy for the transition within the harmonic approximation to transition state theory.

2.3.1   Nudged Elastic Band Method

A widely used method for finding MEPs is the nudged elastic band method (NEB) [18]. The NEB can be used to find an MEP between a pair of local minima on the energy surface [19]. In the context of reaction rates, this pair of local minima represent an initial and a final state. NEB is a chain-of-states method in which a string of images (geometric configurations of the system) is used to describe a reaction pathway. The images are discretization points in the numerical representation of the path. They are connected by spring forces to make them equally spaced along the path [18]. The total energy of such a system is:

$$S^{NEB}\left(R_1, R_2, \ldots., R_p\right) = \sum_{i=1}^{p} V\left(R_i\right) + \sum_{i=1}^{p-1} \frac{k_{sp}}{2}\left(R_i - R_{i+1}\right)^2 \qquad (2.21)$$

The first term is the energy of the individual images and the second is the spring energy that connects the images. The images along the NEB are relaxed to the MEP through a force projection scheme in which only the component of the true force perpendicular to the band is included, and only the parallel component of the spring force is included (the 'nudging') [20].

2.3.2   Climbing Image Nudged Elastic Band

To obtain the saddle point energy and thereby the activation energy of the transition with higher accuracy, a climbing image nudged elastic band (CI-NEB) approach is used. There, the highest energy image along the band is converged to the saddle point to a specified precision. The climbing image moves up the potential energy surface along the elastic band and down the potential surface perpendicular to the band. The climbing image is not affected by the spring forces at all. The climbing image NEB method constitutes a small modification to the NEB method. Information about the shape of the MEP is obtained after a few iterations with the regular NEB. Then, the image with the highest energy is identified [20]. The climbing image does not add any significant computational effort. All the NEB calculations in this thesis were optimized by the climbing image method.

2.4   Computational methods

The DFT calculations were carried out [21] on surfaces of face-centered cubic (FCC) and body-centered cubic (BCC) transition metals. Open surfaces where atoms are not close packed were studied, namely BCC(100) and FCC(100). The BCC metals included V, Fe, Nb, Mo, Ta and W, while the FCC metals included Ni, Cu, Rh, Pd, Ag, Ir, Pt and Au. All calculations involving Ni and Fe atoms include the effect of spin polarization. We did not include hexagonal close packed (HCP) transition metals in this study. The calculations were carried out using the Vienna *ab initio* Simulation Package (VASP) [11] [12] [14] [13] and the RPBE functional approximation [22] [23]. First, the optimal lattice constant for each crystal at zero temperature was found. The following results were obtained: Ta 3.33 Å, V 3.02 Å, Nb 3.33 Å, W 3.20 Å, Mo 3.20 Å, Pd 4.02 Å, Cu 3.71 Å, Ag 4.21 Å, Au 4.22 Å, Rh 3.85 Å, Ir 3.87 Å and Pt 4.02 Å.

All the surface calculations were performed on five layer slabs. A 2×2 unit cell was employed with the three top layers allowed to relax and the bottom two layers kept fixed at the bulk positions. The slab was separated from its periodic images by 13 Å of vacuum. In construction of the potential energy surfaces, one metal atom on the surface of the slabs (the furthest one

from hydrogen atom) was fixed to minimize the large reconstruction that occurred on some of the metals. The potential energy surface was computed by firstly relaxing the clean slabs and then adding the hydrogen atom at various positions on the relaxed surface and relaxing further. For comparison, calculations were also carried out with the whole surface layer fixed (two bottom layers and the upper surface layer were fixed and the two layers in between them were free to move). The first type of configurations will be referred to as 'relaxed slab' and the second type of configuration as 'fixed slab'.

The energy of the system was minimized with respect to the atom coordinates until the highest force in any direction on any movable atom was less than 0.01 eV/Å. The Monkhorst-pack k-points of dimensions 4×4×1 was used to sample the Brillouin zone after a convergence test (see Section 3.1.2) and the valence electrons were represented with a plane-wave basis set with an energy cutoff of 400 eV after the convergence test (see Section 3.1.3).

To calculate the activation energy for diffusion, the CI-NEB method was employed [18] [24]. The activation energy was calculated as the energy of the highest maximum along the MEP minus the initial state energy. The MEP for hops between minima on the potential energy surface of hydrogen on the metal surfaces was calculated using 6 to 12 images in the discrete representation of the path, including the two fixed endpoints. The climbing image was used to determine the saddle points accurately.

For calculating the potential energy surface (PES) of the H-atom on the metal surface, the H atom was placed ca. 1.5 Å above the relaxed metal surface. The x- and y-coordinates of the H-atom were fixed but the z-coordinate as well as the movable metal atoms were allowed to relax so as to minimize the energy. A total of 36 different points in the x-y plane were calculated in this way to form a grid, see Figure 2.1. Symmetry was used to reduce the region sampled to ¼ of the surface unit cell. The same process was repeated for slabs with fixed surface atoms because large relaxations occurred for some of the surfaces.

The adsorption energy of the hydrogen on each point is calculated with the following equation:

$$\Delta E = E_{metal-H} - E_{metal} - E_{H_{2(g)}}/2 \qquad (2.22)$$

Where $E_{metal-H}$ is the total energy of the metal slab with an adsorbed H atom, E_{metal} is the total energy of the clean metal slab and $E_{H_{2(g)}}$ is the total energy of a hydrogen molecule in gaseous state.

1	7	13	19	25	30	31	25	19	13	7	1
2	8	14	20	26	31	32	26	20	14	8	2
3	9	15	21	27	32	33	27	21	15	9	3
4	10	16	22	28	34	34	28	22	16	10	4
5	11	17	23	29	35	35	29	23	17	11	5
6	12	18	24	30	36	36	30	24	18	12	6
6	12	18	24	30	36	36	30	24	18	12	6
5	11	17	23	29	35	35	29	23	17	11	5
4	10	16	22	28	34	34	28	22	16	10	4
3	9	15	21	27	33	33	27	21	15	9	3
2	8	14	20	26	32	32	26	20	14	8	2
1	7	13	19	25	31	31	25	19	13	7	1

Figure 2.1. A 2D grid diagram indicating the points in the x-y plane used for the H atom in order to map out the PES. The dark grey area includes the points calculated by DFT, and the lighter areas contain symmetrically equivalent points, as indicated by the numbering scheme.

Chapter 3

Results and discussion

3.1 Convergence

A number of convergence tests were performed to establish the optimal value of various parameters in the numerical calculations. The results of the tests are described below.

3.1.1 Number of layers

A convergence test was made to determine the number of the layers required in the slab model to obtain converged binding energy. The Pt(100) surface was chosen to represent the FCC transition metals and Nb(100) was chosen to represent the BCC transition metals. The number of the layers was increased until energy was converged to within 0.05 eV . The bottom two layers were fixed and the rest of the layers were allowed to relax. The binding energy of the H adatom interacting with the surface at a bridge site was calculated.

The binding energy of H to each of the metal slabs as a function of number of layers in the slab is shown in Figure 3.1. For Pt(100), the number of layers was increased to 10. The result showed that 5 layers were sufficient to obtain convergence to within 0.05 eV. For Nb(100) slab, the number of the layers was increased to 14 and the adsorption energy was found to change by less than 0.05 eV from 5 layers on. Therefore, 5 layers were deemed sufficient to model the binding of H to metal slabs, for both FCC(100) and BCC(100) transition metals. Furthermore, 5 layers is a computationally feasible model, since the computational time (CPU) time increases as the number of atoms cubed.
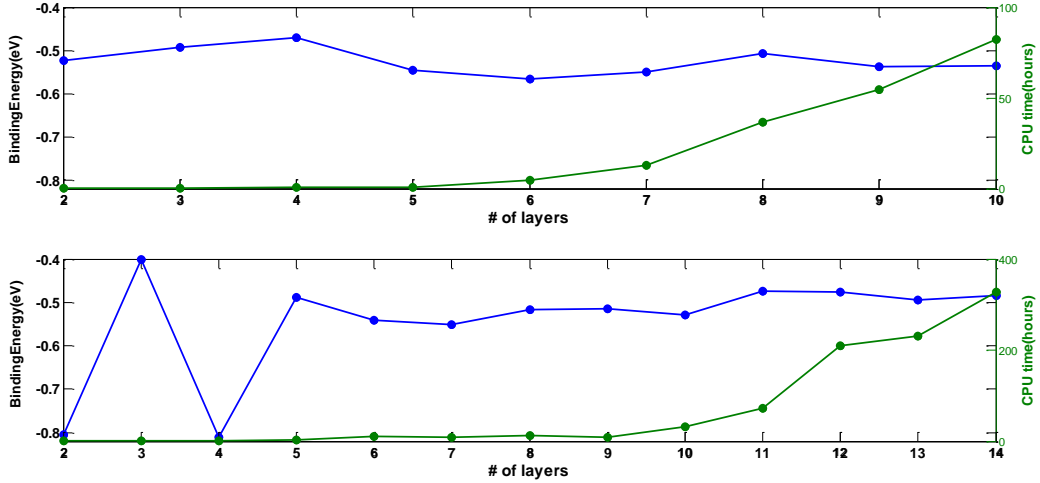
Figure 3.1. H-adatom binding energy as a function of the numbers of the layers and calculated time for Pt(100) (upper figure) and Nb(100) (lower figure).

3.1.2   k-points

A convergence test for k-point sampling was performed for Pt(100) slab with 2×2 surface cell and five layers of metal atoms. The H atom was placed on three different sites: Top, bridge and the four-fold hollow site. The binding energy of the H atom was calculated using various sets of k-points ranging from 2×2×1 to 16×16×1. In each of these cases the plane wave kinetic energy cutoff of 400 eV was used. The slabs were separated by 13 Å of vacuum, the two bottom layers kept fixed and the three upper layers relaxed as the H atom was free to move in x-, y- and z-directions.

 The binding energy of the H atom was calculated on the three sites for each set of k-points and is shown in Figure 3.2. The change in binding energy in going from k-points 4×4×1 to 16×16×1 was found to be between 0.036 and 0.05 eV for all sites. As our interest is mainly on the relative binding energy at the various sites, we focused on the difference in binding energy between these three sites, rather than the absolute value of the binding energy at any of the sites. It can be seen that the differences of binding energy between hollow-bridge and hollow-top changes by only ~0.01 eV when using a k-point sampling of 4×4×1 and larger. Therefore it is concluded that, a k-point set of 4×4×1 is sufficient for this system of a 2×2 simulation cell. It represents a good compromise between accuracy and computational cost.
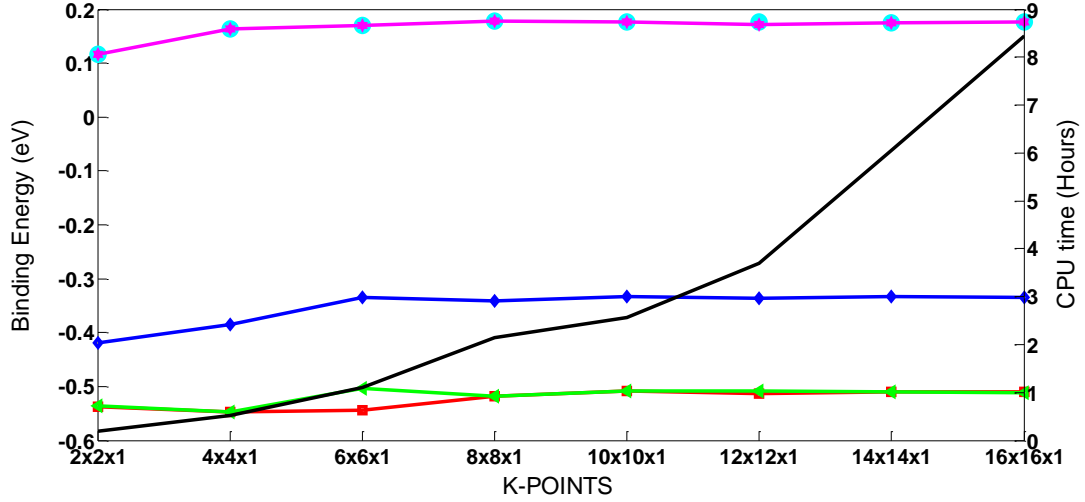
Figure 3.2. The calculated binding energy of H atom on various sites on Pt(100) and associated computational time with different sets of k-points. The red square, blue diamonds and green triangles denote bridge, top and hollow sites, respectively, and the black solid line denotes the computational time, the purple asterisk and light blue circles are the differences in adsorption energy of hydrogen between bridge-top and top-hollow sites, respectively.

3.1.3　Basis set

The convergence of the energy with respect to the plane-wave cutoff was investigated. A test of Pt(100) 2×2 slab with 5 layers was used, the periodic images of the slab separated by 13Å and a Monkhorst-Pack k-point grid of dimensions 4×4×1. All configurations were optimized until atomic forces were less than 0.01 eV/Å. The three uppermost layers in each slab configuration were allowed to relax and the two bottom layers were kept fixed, with atomic distances consistent with the optimal lattice constant. (The optimal lattice constant for Pt crystal at zero temperature was found to be 4.011 Å). [6]

The H atom was placed at a bridge site and the adsorption energy calculated with cut-off energy ranging from 200 to 450 eV, and the results are shown in Figure 3.3.. It was found that the

binding energy varied significantly for the smaller basis set. This is not surprising as a large plane-wave basis set is generally required to describe light atoms. For a plane-wave cutoff of 400 eV and 450 eV, however, the energy was converged to within 0.01 eV. Accordingly, an energy cut-off of 400 eV for the plane wave basis was used in the rest of the calculations.
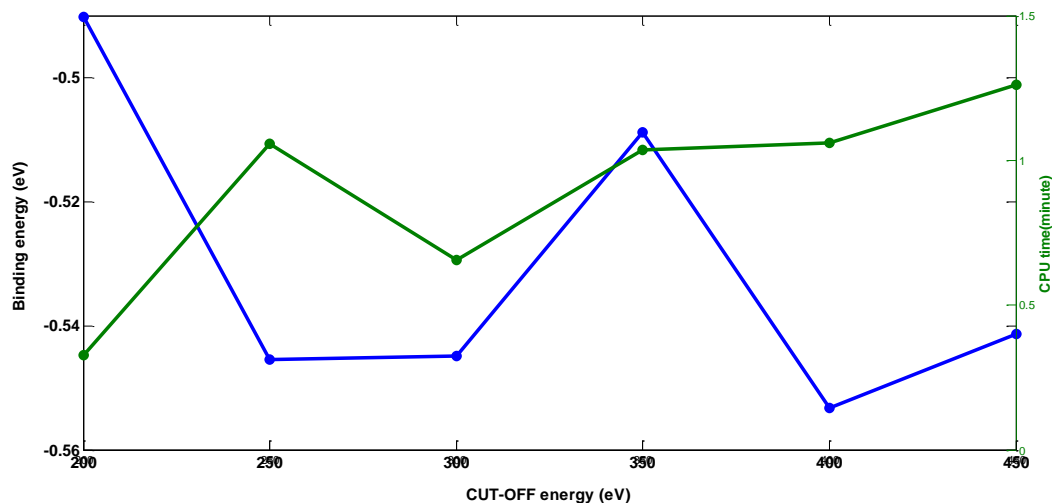
Figure 3.3. Calculated H atom binding energy at a bridge site on Pt(100) surface as a function of the cut-off energy in the plane wave basis set, and the time needed for the calculation.

3.2   Spin-polarized systems

To identify the most appropriate magnetic ordering for the spin-polarized slabs of Fe and Ni that will be used later in this work, several factors must be considered. Firstly, the lattice constant and preferred magnetic ordering of the bulk systems must be calculated. Secondly, the preferred magnetic ordering of the slabs must be determined. Finally, the magnetic ordering in the presence of adsorbed hydrogen must be determined.

3.2.1   Bulk metals

The optimal lattice constant and magnetic ordering was calculated for bulk nickel and iron. The BCC and FCC crystal structures were used for iron and nickel, respectively. For the calculation of the crystal, a plane wave kinetic energy cutoff of 400 eV was used and a Monkhorst-Pack grid of dimensions 6×6×6 was used to sample the Brillouin zone. Simple bulk systems were constructed for the ferromagnetic (FM) and nonmagnetic (NM) systems. Two different antiferromagnetic (AFM) phases were considered, corresponding to two different orientations of the magnetic moments. For nickel, AFM orderings along the (100) and (111) directions were considered. For iron, AFM orderings along the (100) and (110) directions were considered.

The energy of each of the magnetic phases was calculated as a function of lattice constant to determine the optimal lattice constant for a given metal and magnetic phase. These are presented in Fig. 3.4. The essential information is collected in Table 3.1.
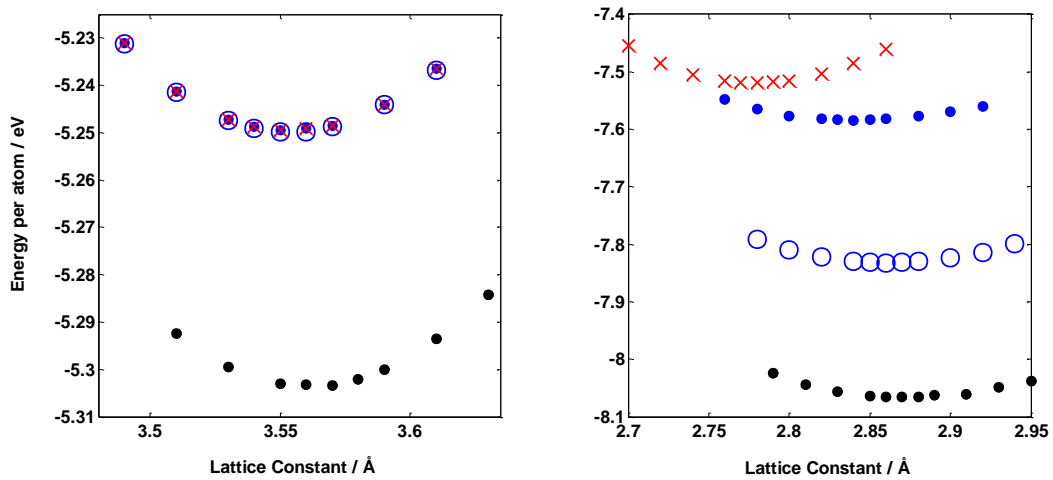
Figure 3.4. Energy as a function of lattice constant for ferromagnetic, antiferromagnetic and nonmagnetic crystals of Ni (left) and Fe (right). The black dots represent ferromagnetic phase, the blue circles represent antiferromagnetic phase and the red crosses represent nonmagnetic phase. Results on slabs are shown with filled blue circles to represent AFM(100) for both metals and empty blue circles to represent AFM(111) for Ni and AFM(110) for Fe.

Table 3.1. Energy (eV) and magnetic moment (μ_B) at the optimal lattice constant for bulk Ni and Fe. ΔE is the energy relative to the lowest energy magnetic phase.

	Ni			
	FM	AFM(100)	AFM(111)	NM
a / Å	3.57	3.55	3.55	3.55
μ_B	0.647	0.000	0.000	0.000
E (eV per atom)	-5.30	-5.25	-5.25	-5.25
ΔE (eV per atom)	0	0.05	0.05	0.05

	Fe			
	FM	AFM(100)	AFM(110)	NM
a / Å	2.87	2.84	2.86	2.78
μ_B	2.321	1.676	2.137	0.000
E (eV per atom)	-8.07	-7.58	-7.83	-7.52
ΔE (eV per atom)	0.00	0.48	0.23	0.55

For Ni, the magnetic moment of the FM phase was found to be 0.647 μ_B and the optimal lattice constant 3.57 Å. This is similar to the experimental values of 3.52 Å [25] and 0.668 μ_B [26]. No AFM solution was found for Ni and all calculations relaxed back to the nonmagnetic solution. The lattice constant of NM and FM Ni differ by only 0.02 Å, which is perhaps not surprising, given the relatively small magnetic moment of FM Ni. FM Ni was found to be lower in energy than AFM and NM Ni and thus it is concluded that bulk Ni is ferromagnetic in the ground state.

For Fe, the lattice constant of the FM phase was found to be 2.87 Å which is in perfect agreement with experimental value of 2.87 Å [27]. The magnetic moment at the optimal lattice constant was found to be 2.32 μ_B, which is in good agreement with both the experimental value (2.22 μ_B) [27] and a previous theoretical estimate 2.17 μ_B [28]. The optimal lattice constant of AFM iron was found to be 2.84-2.86 Å, depending on the orientation of the magnetic moments with respect to the crystal planes. Surprisingly, the energy of the AFM (110) phase was lower in energy than the AFM(100) phase. Additionally, the magnetic moment of the two magnetic phases was rather different (1.676 and 2.137 μ_B for AFM(100) and AFM(110), respectively). A previous calculation yielded a magnetic moment of AFM Fe of 1.25 μ_B [28], which is clearly in better agreement with our AFM(100) phase. Nonmagnetic iron was found to have an optimal lattice constant of 2.78 Å. The energy of the FM phase was found to be around from 0.23-0.5

eV/atom lower than the NM and AFM phases, and thus it is concluded that bulk iron is ferromagnetic in the ground state.

3.2.2   Finite Slabs

To see whether the preferred magnetic ordering is different when a finite slab of metal is used, the energy of slabs of iron and nickel in the ferromagnetic, two antiferromagnetic and nonmagnetic configurations was calculated. For Fe, the AFM(110) ordering has two possible arrangements in a finite slab. The first is denoted "perp", in that of the four surface atoms in the simulation cell have magnetic moments ordered such that two perpendicular nearest neighbors have the same direction of the magnetic moment. The configuration "diag" denotes the AFM(110) case in which the pairs of atoms that are diagonally opposite have the same direction of the magnetic moment. Schematic illustrations of the finite slabs are shown in Fig. 3.5.
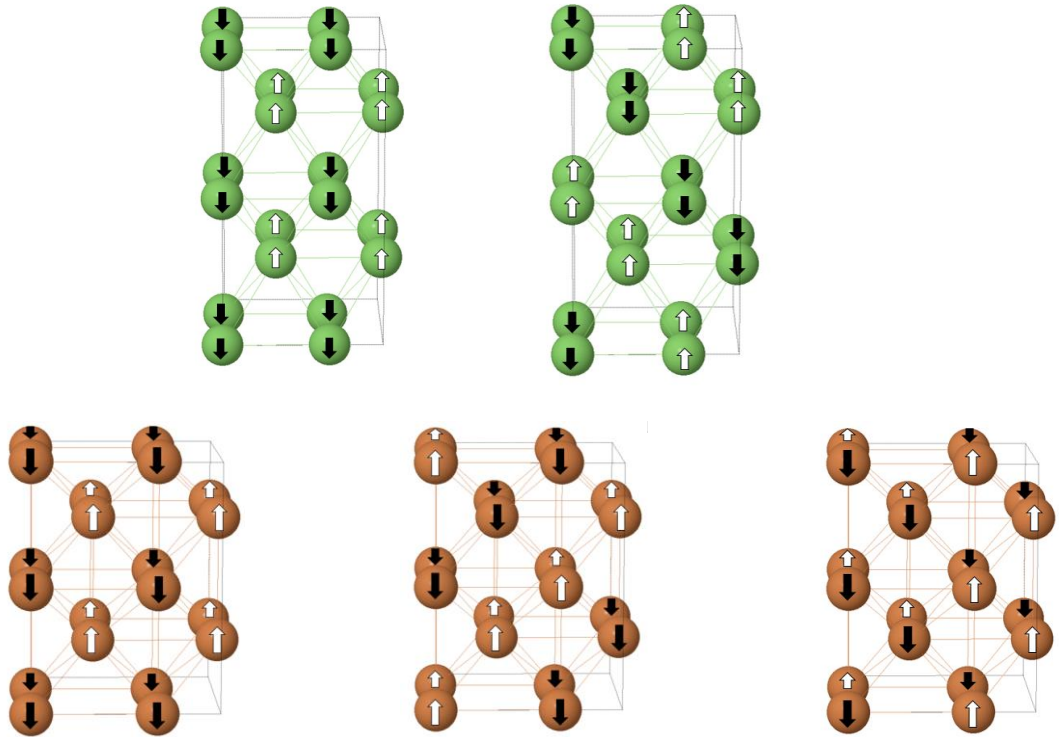

Figure 3.5: Schematic illustrations of slabs of various AFM phases. Top, from left: AFM(100) and AFM(111) for FCC Ni. Bottom, from left: AFM(100) and AFM(110)[perp] and AFM(110)[diag] for BCC Fe.

The energy of each of the slabs was computed at the corresponding optimal lattice constant found in Section 3.2.1. The bottom two layers were held fixed at this lattice constant and the top three layers were allowed to relax. The calculated energy per atom of the slabs of Ni and Fe, as well as the magnetic moments of the surface atoms is presented in Table 3.2.

Table 3.2. Energy (E) and magnetic moment (μ_B) at the optimal lattice constant for finite slabs of Ni and Fe. ΔE is the energy relative to the lowest energy magnetic ordering.

	Ni				
	FM	AFM(100)	AFM(111)		NM
a / Å	3.57	3.55	3.55		3.55
μ_B (surf)	0.796	0.00	0.00		0.00
E (eV per atom)	-4.72	-4.68	-4.68		-4.68
ΔE (eV per atom)	0.00	0.05	0.05		0.05

	Fe				
	FM	AFM(100)	AFM(110)[perp]	AFM(110)[diag]	NM
a / Å	2.87	2.84	2.86	2.86	2.78
μ_B (surf)	2.989	~1.835[a]	2.854	2.871	0.00
E (eV per atom)	-7.65	-7.23	-7.41	-7.44	-7.10
ΔE (eV per atom)	0.00	0.41	0.23	0.20	0.55

[a] The surface of the slab was highly disordered after relaxation. This is an average value of the four surface atoms.

For Ni, the relative energy of the various slabs is similar to the relative energy of corresponding bulk samples. Both AFM solutions relaxed to the nonmagnetic solution, the energy of which was 0.05 eV/atom higher than the FM solution. The magnetic moment of the surface layer of the slab was slightly larger than the bulk (0.796 μ_B compared to 0.647 μ_B).

For Fe, the relative energy difference between the various magnetic phases is also essentially the same as for the crystal samples. A slight difference is that the AFM(100) magnetic ordering is slightly favored in a slab, however the energy difference is small. This surface showed significant rearrangement after relaxation. Accordingly, the magnetic moment showed

significant variation between the surface atoms but the average value was 1.835 μ_B, which is slightly higher than the magnetic moment of the same ordering in the crystal. For both of the AFM(110) phases, as well as the FM phase, the magnetic moment of the surface atoms is significantly larger than in the bulk. It should be noted at this stage that it is very difficult to converge the solutions of magnetic moments in finite slabs and the precise values of these should be treated with caution. Regardless, it is obvious that for Fe the ground state magnetic ordering when it is a finite slab remains strongly ferromagnetic, as for the crystal.

3.2.3   Finite Slabs with adsorbed hydrogen

The energy surfaces representing the interaction of a H atom with the metal surfaces was then calculated. Of particular interest is whether the presence of the H atom at the surface has any effect on the preferred magnetic ordering and the magnetic moment of the surface metal atoms. The binding energy of a hydrogen atom on Fe and Ni slab (as referred to in previous section (3.2.2)) surfaces was calculated. Hydrogen was placed above a bridge site (see figure 3.6) of the surface. All the various magnetic phases were considered. The relative energy of the slabs with adsorbed hydrogen, as well as the magnetic moment of the surface metal atoms is given in Table 3.3.

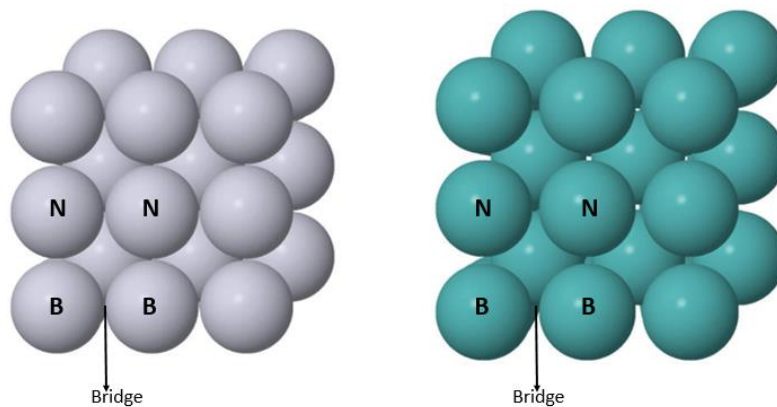**Figure 3.6** An illustration of the bridge site for adsorbed H-atom on BCC(100) [left] and FCC(100) [right] surfaces. The label N refers to a metal atom to which the H atom does not bind, while B refers to a metal atom which the H atom binds to.

Table 3.3. Energy (E) and magnetic moment (μ_B) at the optimal lattice constant for finite slabs of Ni and Fe with a hydrogen atom adsorbed on the bridge site. 'H-binding' and 'not H-binding' refer to the surface metal atoms participating and not participating in the bonding to the H atom, respectively. ΔE is the energy relative to the lowest energy magnetic ordering. Note that the energy is per *metal* atom.

	Ni				NM
	FM	AFM(100)	AFM(111)		NM
a / Å	3.57	3.55	3.55		3.55
μ_B (H-binding)	0.569	0.00	0.00		0.00
μ_B (not H-binding)	0.804	0.00	0.00		0.00
E (eV per Ni atom)	-4.92	-4.87	-4.87		-4.87
ΔE (eV per Ni atom)	0.00	0.05	0.05		0.05

	Fe				
	FM	AFM(100)	AFM(110)[perp]	AFM(110)[diag]	NM
a / Å	2.87	2.84	2.86	2.86	2.78
μ_B (H-binding)	2.830	~1.850	2.739	2.783	0
μ_B (not H-binding)	2.978	~1.925	2.854	2.861	0
E (eV per Fe atom)	-7.83	-7.43	-7.60	-7.63	-7.30
ΔE (eV per Fe atom)	0.00	0.40	0.23	0.20	0.53

The relative energy of the Ni slabs with adsorbed hydrogen of various magnetic phases show the same trends as the slabs without the H atom. Once again, no AFM solution is found and the FM solution is the most stable. It is interesting to note that the magnetic moment of the surface atoms is similar to the clean slabs except for the metal atoms directly involved in the bonding to the H atom. For these metal atoms the magnetic moment is lowered.

In general, the magnetic moments of the Fe atoms in the slabs with adsorbed H atom are slightly lower than the clean slabs. Once again, the two metal atoms that are bridged by the H atom have a consistently lower magnetic moment than the other two surface metal atoms. This is the case for all of the magnetic phases considered. As for the energy, once again little change is seen compared with the crystal and, once again, the FM ordering is seen to be the most stable. We can see how the reactivity of the metal surfaces can be affected significantly by changing the magnetic state.

The energy of different magnetic orderings were calculated for Ni and Fe crystal, slab and the slab with hydrogen, and it was found in all cases that the ferromagnetic phase (FM) is the most stable one for both Ni and Fe. Therefore, the FM phase was chosen for the Ni and Fe slabs in the rest of this study. The presence of H on the surface of the slabs was found not to alter the preferred magnetic ordering and only reduce the magnetic moment of the surface metal atoms slightly.

3.3 Potential Energy Surfaces for H Atom

The Sabatier principle [29] is one of the oldest rules in catalysis. For a two-step reaction passing through an adsorbed intermediate, such as the hydrogen evolution reaction, it states that the adsorption free energy should be neither too high nor too low. If the Sabatier principle is the only factor that governs a reaction, a plot of the reaction rate versus the free energy of adsorption of the intermediate results in a volcano curve [30]. If an adsorbate binds too strongly then it is difficult to remove the product from the catalyst. Conversely, if an adsorbate does not bind strongly enough, the reaction does not occur readily. These two considerations give rise to the ascending and descending legs of the volcano curve, respectively [31].
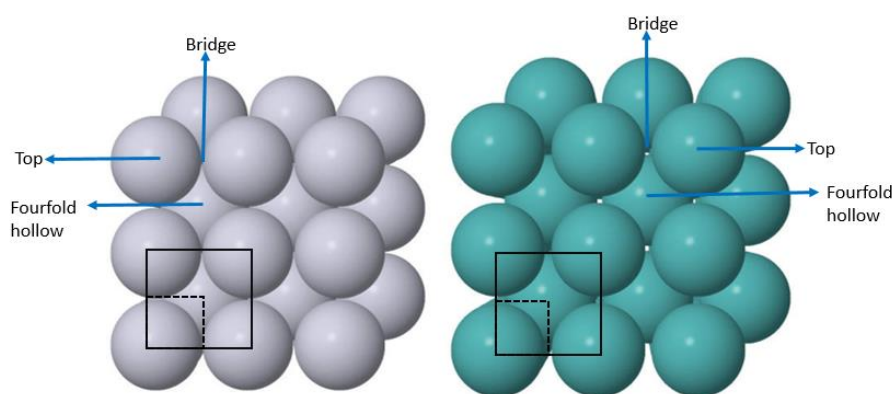

Figure 3.7: The structure of BCC(100) [left] and FCC(100) [right] metal surfaces. The box (dashed line) shows the area where the H atom was placed. The box (solid line) shows the area of the surface unit cell. The arrows indicates the three types of sites: Top, bridge and fourfold hollow.

Potential energy surfaces (PESs) representing the interaction of a H atom with various transition metals surfaces, FCC(100) and BCC(100), relative to H_2 in the gas phase, were computed using DFT as described above. Fig. 3.7 shows the regions of the surfaces calculated and the PESs themselves are shown in Fig. 3.8. The PESs can be used, for example, to assess whether or not a metal is likely to be a good hydrogen evolution catalyst according to the Sabatier principle. At the equilibrium potential the metal is a good hydrogen formation catalyst when the free energy of adsorption of hydrogen from solution is close to zero. The free energy of adsorption at atmospheric temperature and pressure can be estimated from the energy of adsorption by shifting the energy up by 0.2-0.25 eV to account for zero point energy and entropy effects (mainly the entropy loss as the gas phase molecule adsorbs on the surface) [33] [34]. Thus, the best H_2

evolution catalyst has an adsorption energy of between -0.2 and -0.25 eV.

3.3.1 PES for H atom on FCC(100) and BCC(100) metal surfaces

The PES of hydrogen was computed on various transition metals relative to H_2 in gas phase. Figure 3.8 shows the adsorption energy of hydrogen on selected metals with both relaxed and frozen configuration. The purpose of the frozen configuration is to simplify the problem and investigate the binding in the absence of metal atom relaxation. We will begin discussion with the relaxed surfaces. It can be seen that the best H_2 evolution catalysts are from Groups 9, 10 and 5. On these surfaces, the hydrogen atoms binds with an energy of around -0.2 to -0. 5eV while the noble metals bind the H atom too weakly and the remaining metals of this group bind the H atom too strongly.

In general the most stable adsorption sites are at the bridge and fourfold hollow sites except for Ir(100) and Pt(100), where the top site is the next favorable adsorption site after bridge site. The bridge site is favored for hydrogen adsorption by 0.05 and 0.18 eV for Ir(100) and Pt(100), respectively.

The distance between the H atom and the surface plane is largest at the top site, then at the bridge site, and shortest at the fourfold hollow site. The binding energy at the fourfold hollow site is between 0.34 eV and 0.57 eV, which agrees with previous calculations which gave 0.38 eV to 0.63 eV. [32]. The hydrogen-surface atom distance is also in good agreement, for all surfaces in this thesis.

As stated previously, the noble metas Cu, Ag and Au bind hydrogen too weakly to be good hydrogen evolution catalysts. These metals are significantly separated from the other metals.. The next lowest binding energy is on Fe(100), which binds hydrogen more strongly than the strongest-binding noble metal surface by 0.19 eV [32].
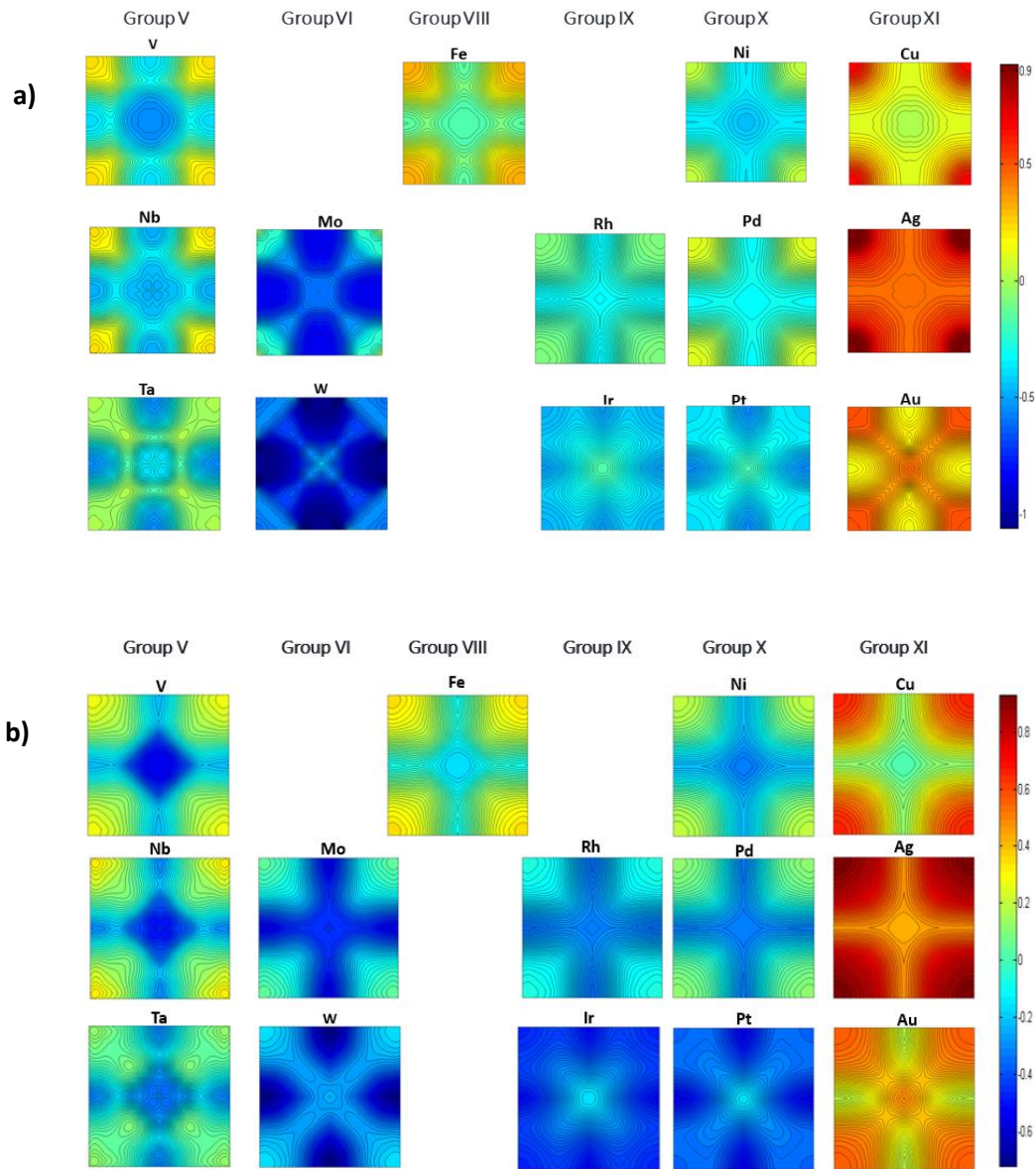
Figure 3.8. The PES of hydrogen on selected metals relative to H_2 in gas phase of (a) relaxed surface and (b) fixed surface.

Ni(100) and Fe(100) with adsorbed H atom have magnetic moments of 0.62 and $2.7\mu_B$ per metal atom respectively which is close to the calculated value 0.6 and $2.7\mu_B$ for Ni(100) and Fe(100) respectively [32]. The favorable site for Pd and Rh is bridge site with a little difference with fourfold hollow site 0.008 and 0.030 eV for Pd and Rh respectively, where the fourfold hollow site was found to be favorable for Pd and Rh in a previous study [32]. The on top site usually has a higher binding energy and this difference is greater in metals within group 5 and 6 which is around 0.42 to 0.8 3eV.

The values mentioned above were for frozen surfaces. When the relaxation of surface metal atoms was included, some of the metals such as V, Nb, Ta, Mo and W showed large displacements of the metal atoms, sometimes by more than 0.45 Å.

The biggest difference in the PES between the relaxed and frozen surfaces was obtained for the surfaces where the biggest relaxation occurred. Table 3.4 lists the adsorption energy of the H atom at top, bridge and fourfold hollow sites. Fixing the surface atoms did not change the binding qualitatively. For instance, the strongest binding was obtained in the same sites irrespective of whether relaxation was included or not. Visual inspection of the PES of the H atom at the metal surfaces shown in Figures 3.8(a) and 3.8(b) shows the same pattern. It can be seen that the binding is stronger when relaxation of the surface atoms is included. The system necessarily uses the additional degrees of freedom to lower the energy.

Table 3.4. The binding energy of hydrogen on fixed and relaxed surface metals of top, bridge (bri) and fourfold hollow (hol) sites, all the values are in (eV).

Metal	Top (relaxed)	Top (fixed)	Bridge (relaxed)	Bridge (fixed)	Hollow (relaxed)	Hollow (fixed)
Ag	0.92	0.93	0.46	0.47	0.45	0.45
Au	0.53	0.57	0.15	0.18	0.48	0.50
Cu	0.68	0.68	0.13	0.14	0.01	0.02
Fe	0.35	0.35	-0.15	-0.09	-0.17	-0.17
Ir	-0.47	-0.47	-0.52	-0.52	-0.16	-0.15
Mo	0.00	0.03	-0.84	-0.56	-0.57	-0.42
Nb	0.21	0.28	-0.49	-0.30	-0.43	-0.42
Ni	0.06	0.20	-0.37	-0.22	-0.45	-0.33
Pd	0.12	0.12	-0.32	-0.32	-0.32	-0.32
Pt	-0.38	-0.36	-0.55	-0.54	-0.17	-0.15
Rh	-0.07	-0.07	-0.35	-0.35	-0.32	-0.31
Ta	0.01	0.10	-0.56	-0.32	-0.30	-0.28
V	0.24	0.29	-0.40	-0.22	-0.55	-0.54
W	-0.59	-0.16	-1.05	-0.71	-0.44	-0.22

The H atom PESs obtained in this research for the more open surfaces can be compared with the PES obtained for closed packed transition metal surfaces FCC(111) and BCC(110) in a previous study [6]. The results are relatively similar except for W, Ta, Mo and Fe, where the difference in binding energies between the open and cloe-packed surfaces is between 0.12 to 0.22 eV.

The difference between the relaxed and fixed PES is investigated in more detail herein. To identify regions of the metal surface for which relaxation of the surface atoms has the largest effect on the binding energy of hydrogen, the difference in H binding energy between the frozen and relaxed surfaces is plotted in Figure 3.9 .
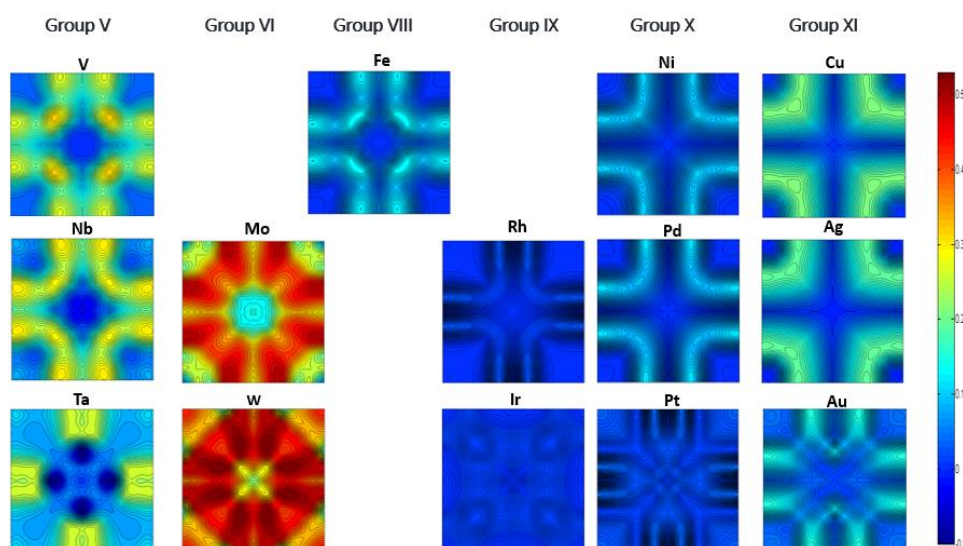
Figure 3.9 The difference in the PES for a H atom on a frozen and relaxed metal surface (relative to H_2 in gas phase).

As can be seen from Figure 3.9, the biggest change in the PES is not occuring at any of the adsorption minima (top, bridge or fourfold hollow sites), but rather near the top site and tilted a bit towards the bridge or the hollow site. This can be seen in the highlighted area in figure 3.10(a). Figure 3.10(b) shows the average relaxation that occurs on these. The biggest relaxation is also for these "tilted top" sites, in accordance with the difference in the PESs..

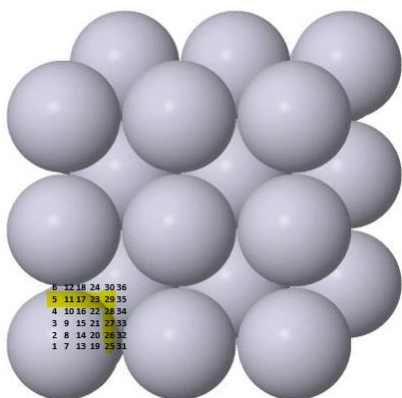**Figure 3.10(a):. T**he highlighted numbers are those positions were the large translation with the surface atoms is happening named as top-tilted.
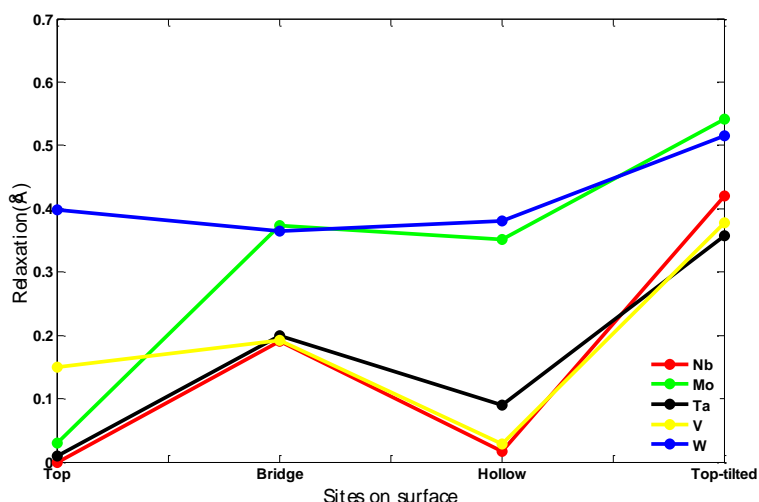
Figure 3.10(b): The relaxation of the surface atoms during the calculations of the binding of the H atom on relaxed Nb, Mo, Ta, V and W slabs.

3.3.2 NEB calculations

An initial estimation of the minimum energy path (MEP) for hydrogen diffusion can be made based on the PES. This can then be refined by calculating the MEP explicitly, using climbing image nudged elastice band (CI-NEB). Figure 3.11 shows the PES of H adatom on selected transition metal surfaces with the minimum set to zero separately for each surface. The lower the binding energy is at the minimum, the lower the energy barrier is and thus the hydrogen diffuses more easily. For most of the metals, the hydrogen difusses by hopping between bridge sites through the fourfold hollow site or from fourfold hollow sites through the bridge sites, except for Ir and Rh where the top site is the second most stable site on the surface and the diffusion takes place on bridge sites through the topsite. The activation energy barriers in general are low, between 0.02 and 0.36 eV.
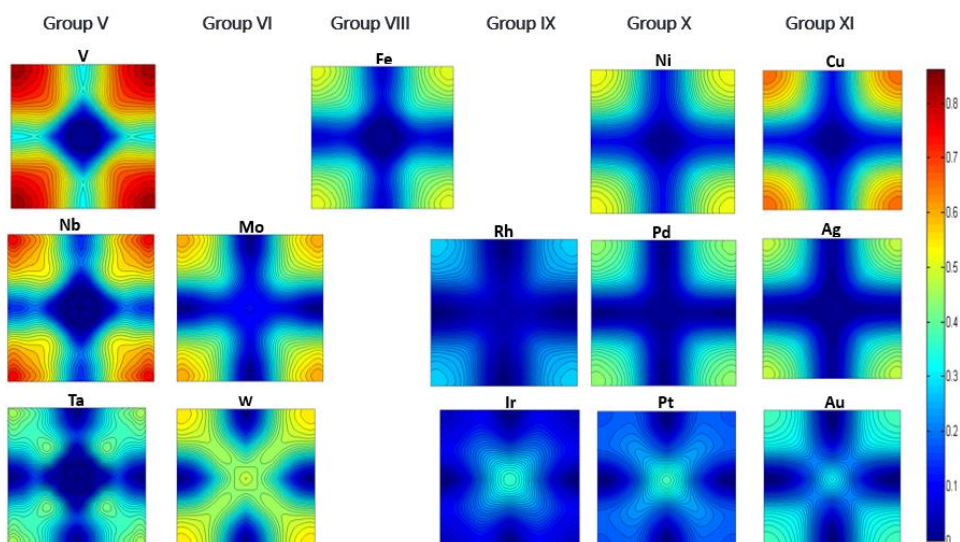
31

Figure 3.11: The PES of transition metals scaled from 0 eV for each metal.

The transition metals from Group 5 and 6 have the highest energy barrier for H diffusion. Pd, Rh, Nb, Au, Mo, Ta and W have the lowest binding energy at bridge sites and the next lowest binding site is the on fourfold hollow site. The diffusion hop takes the H atom from a bridge site through a fourfold hollow site where the saddle point is obtained. Exceptions are W, Mo and Au where the range difference binding energy is rather large between bridge and foufold hollow site, from 0.32 to 0.49 eV, and the MEP goes through the neibouring bridge.

The diffusion of hydrogen on Pt(100) and Ir(100) surfaces involves hops from bridge sites through top sites where the difference in energy is very small. Ag, Cu, Ni, Fe and V have strongest binding of the H atom at fourfold hollow sites and the next strongest binding is obtained at bridge sites. So, the H atom diffuses from fourfold holllow sites throughout the bridge (all the data and the figure of the sites where the hydrogen diffusion is taking place are shown in detail in Appendix).

Since the difference between two energy minima is small for some of the transition metals such as Pd, Ag, Rh, Fe and Ir, the lowest energy path of H diffusion is rather long, rather than being the shortest distance between the initial and final sites. For example, Figure 3.12. shows the MEP calculated by NEB method for three different sites on Ir surface. It can be seen that H diffuses from a bridge site, to a top site then to an adjacent bridge site, rather than through the hollow site. This feature was seen on some of the other metals.
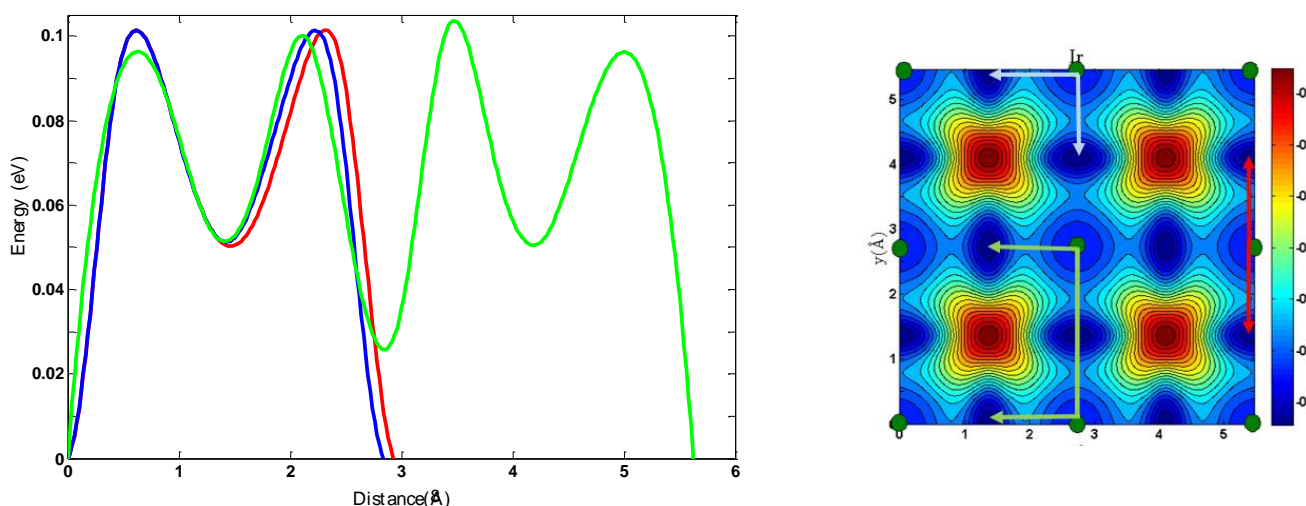
Figure 3.12. (Left) The minimum energy path of hydrogen on Ir(100) between various sites. The red line denotes the path from bridge to another bridge site through a top site. The blue line denotes the path from bridge site to neighbor bridge site which is diagonal to it. The green line denotes the path from bridge site to another bridge throughout a hollow site. (Right) The PES of Ir(100), the arrows show the hydrogen diffusion path for bridge to another bridge site throughout the top site, bridge to neighbor diagonal bridge and bridge to bridge through fourfold hollow site which, represented by red, blue and green arrows respectively. The green filled circles indicating the positions of the Ir surface atoms.

The activation energy decreases when going to the right within the d-block in the periodic table. The highest activation energy is from Group 5 and 6 except for Nb, which is coming after Au, see Figure 3.13(a). Since the difference range of the energy barrier is small we will not attempt to correlate it with the d-band energy.

The adsorption energy of hydrogen at bridge sites is shown in Figure 3.13(b). We can see how the metals tend to have stronger binding energy as they lie farther to the left in the periodic table.
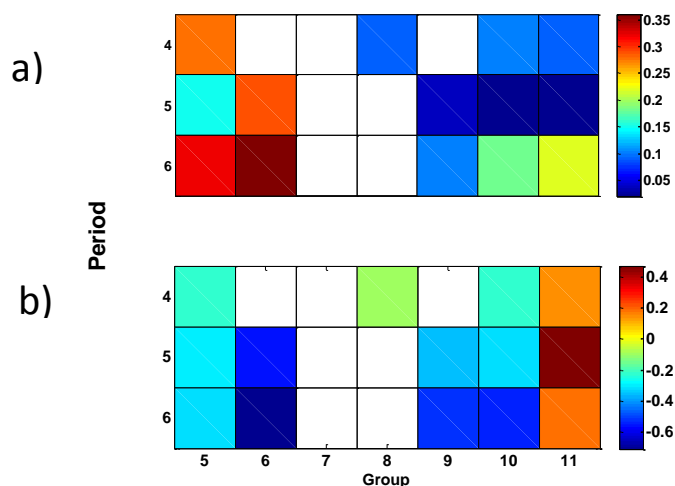
Figure 3.13: (a) The activation energy (eV) for hydrogen atom on the selected metals on periodic table as shown the number of the period and group of periodic table. (b) The adsorption energy (eV) of the bridge site for the H atom on the selected transition metals, each metal is represented by its position in the periodic table.

The activation energy was calculated from the potential energy surface as well as NEB method for the metals considered here and the difference is within 0.02 eV, so the estimation between NEB and PES is excellent. Figure 3.14 shows an example of activation energy for Au(100) and Ir(100) which were obtained with both PES for both relaxed and frozen surfaces and NEB method.
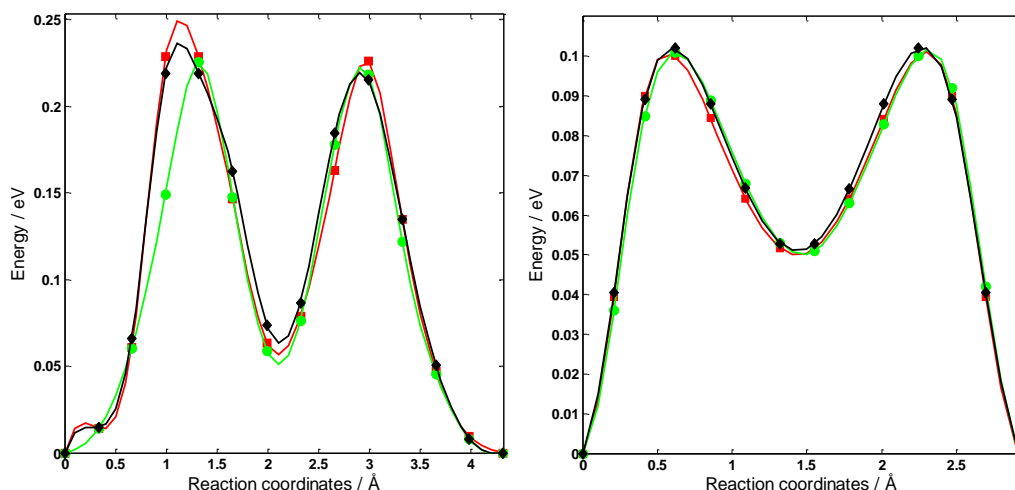
Figure 3.14. Right (Au) and left (Ir), green circles denote the activation energy that obtained from NEB method while the red squares denote the activation energy that obtained from PES of hydrogen on relaxed metal slabs and the black diamonds are the activation energies that obtained from PES of fixed metal slab calculations at specific coordinates in x and y directions of the H adatom, consistent with the position of H from the NEB calculations.

In general, the lower the difference between two energy minima is, the lower the energy barrier will be. To check this rule of thumb, we calculated the difference between the two minima on the surface of each metal and compared it with the activation energy and we found a good correlation, as in Figure 3.15.
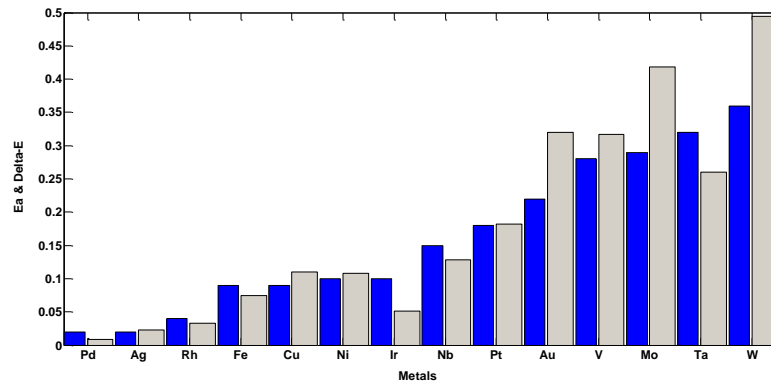

Figure 3.15. The activation energy (blue bars) and the difference between the two minima of PES (grey bars) of the metals both in (eV). The data of this figure is in the table 3.5.

The difference between these two values, the activation energy and difference between two minima (the lowest and next lowest PES) is correlated except for Ir as we see the difference is rather little. As the difference between the lowest binding energy of H atom and highest binding energy on the considered transition metals was compared with activation energy and adsorption energy of hydrogen on the metals, but no correlation was found.

The activation energy of the metals in this study was compared with activation energy of the same group of the metals but with closed packed facets, i.e. FCC(111) and BCC(110) surfaces [6]. No correlation was found between them.

Table 3.5. Comparison of the activation energy of the metals and the difference of the two PES minima where the hydrogen diffuson is occuring..

Metal	Ea (eV)	Delta_E (eV)
Pd	0.02	0.01
Ag	0.02	0.02
Rh	0.04	0.03
Fe	0.09	0.07
Cu	0.09	0.11
Ni	0.1	0.11
Ir	0.1	0.05
Nb	0.15	0.13
Pt	0.18	0.18
Au	0.22	0.32
V	0.28	0.32
Mo	0.29	0.42
Ta	0.32	0.26
W	0.36	0.49

Conclusion

The binding energy of an H atom on the surface of 14 transition metals has been studied using periodic, self-consistent DFT-GGA calculations. The favorable adsorption sites and adsorption geometries were found, as well as the mechanism and activation energy for diffusion. The activation energy is in general very low, from 0.02 to 0.36 eV. The minimum energy path that is obtained from NEB method was compared with the estimate obtained from the PES and the agreement was good. Ag(100) has the lowest energy barrier since the energy landscape is quite flat on its surface. We can see some trends in that the activation energy get higher when moving to the left of the periodic table. The strongest binding energy is obtained on bridge sites on W, Mo, Au, Nb, Pt, Ir, Rh and Pd surfaces while the strongest binding energy is on hollow site on V, Ta, Fe, Ni, Cu and Ag surfaces.

The optimal lattice constant was determined for Ni and Fe in the various magnetic phases, and the rest of the calculations were done based on the lowest energy phase. Various magnetic phases were investigated for the bulk metals, finite slabs and the slab with hydrogen on bridge site for both Ni and Fe. In all cases the ferromagnetic phase was found to be the most stable magentic configuration. The magnetic moment was computed in all cases and was found to be significantly larger on the slab than in bulk for both Ni and Fe. The presence of a H atom on the slab has no effect on the preferences for the magnetic phase and the magnetic moment of the surface metal atoms decreases only slightly by 0.16 and 0.22 μ_B for Fe and Ni respectively in FM orderings.

Due to a large relaxation during the calculations of the PES of some of the metals, in particular V, Nb, Ta, Mo and W, calculations with frozen surfaces were also carried out and the results compared with those obtained for relaxed surfaces. The largest relaxation was occuring when the H atom was placed ner top sites displaced towards bridge or fourfold hollow sites.

Bibliography

[1]   K. Christmann, *Surf. Sci. .,* p. Rep. 9 , (1988) .

[2]   E. S. H. J. . Gudmundsdóttir, *Phys. Rev. Lett. ,* p. 156101, (2012).

[3]   C.N. Satterfield, "Heterogeneous Catalysis in Industrial Practice,," *Krieger Publishing Company, Malabar, FL, ,* p. 2nd ed. , 1996..

[4]   John Wiley, ".A. Somorjai,," *Introduction to Surface Chemistry and Catalysis, ,* 1996.

[5]   W. Kohn, "Rev. Mod. Physic," no. 71, p. 1253, 1999.

[6]   E. S. Lilja Kristinsdóttir, "A systematic DFT study of hydrogen diffusion on transition metal surfaces," *Surface Science,* p. 5, 2012.

[7]   J. A. Pople, "Rev, Mod, Phys," vol. 1267, no. 71, 1999.

[8]   W. Kohn and L. J. Sham, *Phys. Rev,* p. A1133–A1138., 1965.

[9]   K. B. M. Ernzerhof J. P. Perdew, " Generalized gradient approximation made simple," *Phys. Rev. Lett,* vol. 77, p. 3865–3868, 1996.

[10] J. P. Perdew, "in Electronic Structure of Solids, edited by P. Ziesche and H. Eschrig," *Akademie Verlag, Berlin, ,* 1991.

[11] G. Kresse and J. Hafner, *Phys. Rev. B 47, ,* vol. B, no. 47, p. 558, 1993.

[12] G. Kresse and J. Hafner, *Phys. Rev. ,* vol. B, no. 49, p. 14251, 1994.

[13] G. Kresse and J. Furthm•uller, *Comp. Mater. Sci. ,* vol. 6, p. 15, 1996.

[14] G. Kresse and J. Furthm•uller, *Phys. Rev. ,* vol. B, no. 54, p. 11169, 1996.

[15] B. T. a. B. Wavefunctions.

[16] D. Vanderbilt, *Phys. Rev.,* vol. B, no. 41, p. 7892, 1990.

[17] L. M. F. F. C. 3.Duo, " Magnetic Properties of Antiferromagnetic Oxide Materials.," *KGaA, Weinheim: Wiley-VCH Verlag GmbH & Co.,* 2010.

[18] G. M. ,. K. W. J. by Hannes Jónsson, "Nudged Elastic Band Method for Finding Minimum Energy Paths of Transitions," *in Classical and Quantum Dynamics, edited by B. J. Berne, G. Ciccotti,,* 1998.

[19] R. T. a. G. H. Daniel Sheppard, "Optimization methods for finding minimum energy path," *HE JOURNAL OF CHEMICAL PHYSICS ,* no. 128, p. 134106, 2008.

[20] B. P. U. a. H. J. G. Henkelman, "J. Chem. Phys.," no. 113, , 9901.

[21] B. P. U. H. J. Graeme Henkelman, "A climbing image nudged elastic band method for finding saddle points," *JOURNAL OF CHEMICAL PHYSICS ,* vol. 113, no. 22, p. 9901, 2000.

[22] K. W. N. lecture:, "electronic structure of matter wave functions and density functional," *Rev Mod Phys,* vol. 71, no. 1253, 1998.

[23] "RPBE," *Phys. Rev.,* vol. B, no. 59, p. 7413, 1999.

[24] H. L. N. J. (. I. a. Hammer B, " Improved adsorption energetics within density-functional theory using revised Perdew Burke-Ernzerhof functionals.," *Phys Rev ,* vol. B , no. 46, p. 7413, 1999.

[25] B. P. U. H. J. Graeme Henkelman, "A climbing image nudged elastic band method for finding saddle points," *OURNAL OF CHEMICAL PHYSICS ,* vol. 113, no. 22, p. 9901, 2000.

[26] F. a. P. B. Philipp Haas, "Calculation of the lattice constant of solids with semilocal functionals.," *PHYSICAL REVIEW ,* vol. B, no. 79, p. 10, 2009.

[27] F. GALPERIN, "The Electronic Structure and Magnetic Moment of Fe, Co, and Ni Atoms.," *phys. stat. sol. , ,* vol. b(57), p. p. 4., (1973) .

[28] G. a. D. T. W. Zhong, "Structural properties of Fe crystals.," *PHYSICAL REVIEW B,, ,* vol. 47, no. 1, p. 5., 1 January 1993. .

[29] E. a. P. E. H. C. Herper, "Ab initio full-potential study of the structural and magnetic phase stability of iron.," *PHYSICAL REVIEW ,* vol. B 79. , no. 60(6), p. 10, 1999.

[30] F. L. Sabatier, "catalyse en chimie organique," *Berauge: Paris,* 1920.

[31] G. J. R. T. B. J. G. H. J. a. J. E. Skúlason, *Phys.Chem.Chem.Phys,,* vol. 9, p. 3241, 2007.

[32] 2. F. J. E. S. a. W. S. Paola Quaino1, "Volcano plots in hydrogen electrocatalysis – uses and abuses," *Beilstein J. Nanotechnol,* no. 5, p. 9, 2014.

[33] M. M. J. Greeley, *J. Phys. Chem. ,* vol. B , no. 109, p. 3460, (2005) .

[34] V. J. R. T. B. H. J. J. N. E.Skúlason, *J. Phys. Chem. ,* vol. C , no. 114 , p. 18182, (2010) .

[35] S. K. A. U. N. M. M. Peter Ferrin, "Hydrogen adsorption, absorption and diffusion on and in transition metal surfaces," *Surface Science,* vol. 606, p. 679, 2012.

Appendices

List of figures and tables in Appendices

Appendix A. The activation energy barrier for hydrogen diffusion on the selected transition metals, the positions of initial and final point of the reaction path, the relaxation of the surface atoms, position of the saddle point and energy barrier and the lowest adsorption point on the surface.

Metal	NEB_position	Saddle point (eV)	energy berrier	relaxation	difussion	energy barrier	lowest site
W	bri_bri_opp_hol	0.036	0.36	0.28x 0.129y	On bridge	between hol_top	bridge
Ta	bri_bri_opp_hol		0.32	0.24x 0.074 0.117z	hollow	beside next bridge	bridge
Mo	bri_bri_opp_hol	0.076	0.29	0.56x 0.4y 0.061z	beside next bridge	hollow	bridge
V	hol_hol_opp_bri	0.148	0.28	0.16x 0.024y	bridge	between hol_bridge	hollow
Au	bri_bri_opp_hol	0.059	0.22	little	between_bri_hol	between hol_top	bridge
Nb	bri_bri_diagonal	0.050	0.19	little	hollow	between bri_hol	hollow
Pt	bri_bri_diagonal	0.163	0.18	very little	Top	between hol_bridge	bridge
Nb	bri_bri_opp_hol	0.050	0.15	around 0.14A	hollow	between bri_hol	hollow
Ni	hol_hol_opp_bri		0.10	very little	bridge	bridge	hollow
Ir	bri_bri_opp_top	0.053	0.10	very little	top	between _bri_top	bridge
Cu	hol_hol_opp_bri		0.09	very little	bridge	between bri_top	hollow
Fe	hol_hol_opp_bri	0.022	0.09	little	bridge	between_hol_bridge	hollow
Rh	bri_bri_diagonal	0.035	0.04	very little	hollow	between bri_hol	bridge
Pd	bri_bri_opp_hol	0.005	0.02	very little	hollow	between hol_bridge	bridge
Ag	hol_hol_opp_bri	0.015	0.02	very little	bridge	between hol_bridge	hollow

Appendix B. The positions of the final and initial points of the NEB calculations, the black arrow indicates bri_bri_diagonal, the red arrow indicates bri_bri_opp_hol and the green arrow indicates hol_hol_opp_bri mechanism of a diffusion hop.
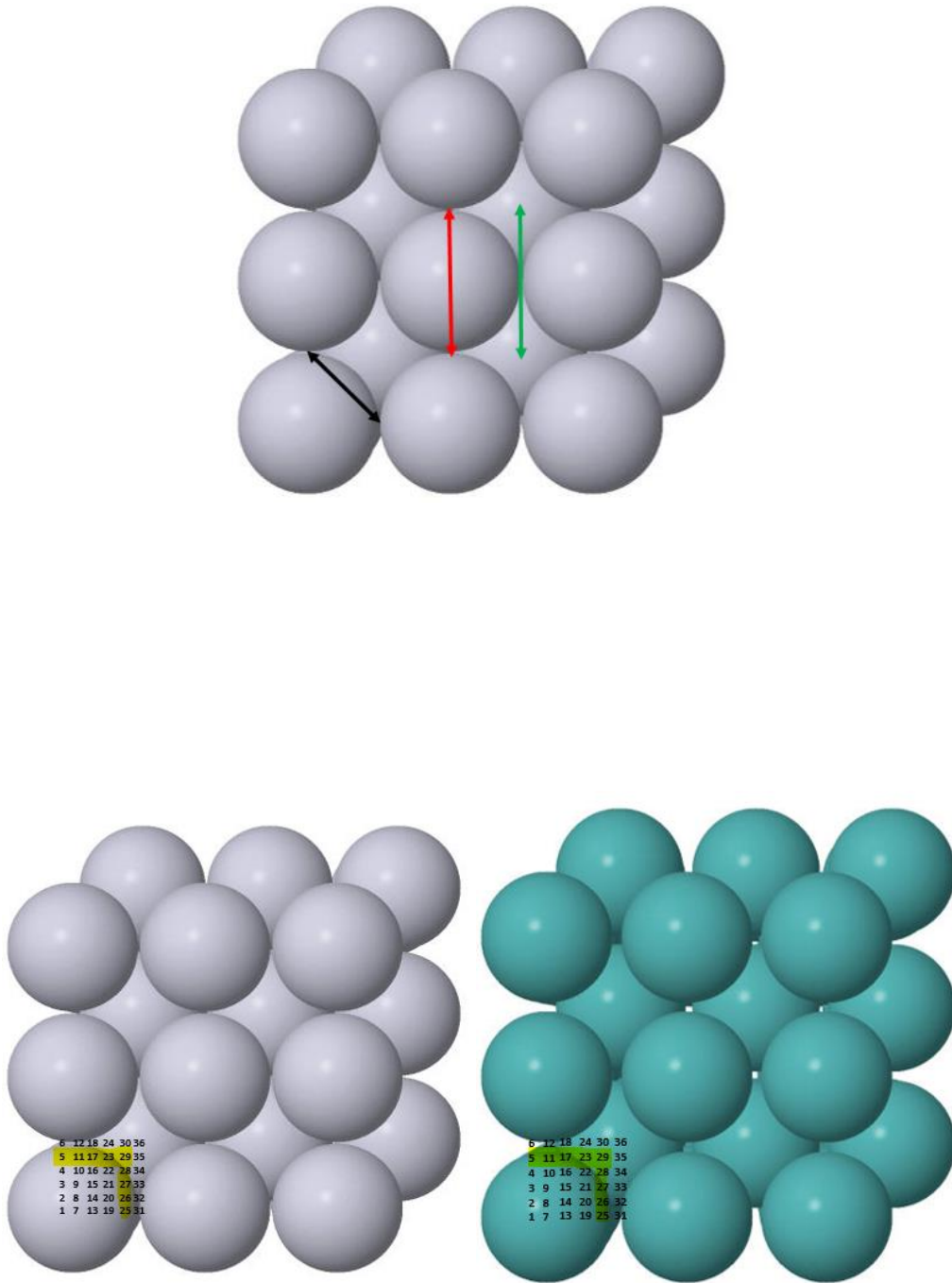
Appendix C. The atomic structure of BCC(100) [left figure] and FCC(100) [right figure] surfaces. The numbers label the x-y positions of the H-atom in the DFT calculations. The highlighted numbers are the positions were large relaxation of the surface atoms occurs.

Appendix D. The reconstruction on surface atoms when hydrogen is interacting with the relaxed metal surface on different sites on x, y and z axes, (the numbers in the second column refers to the position of hydrogen atom on the metal slab (see figure 1.4.), the last column is the difference in PES between relaxed and fixed surface.

The Metal_H	# of positions	Δx (Å)	Δy (Å)	Δz (Å)	Δ energy (Å)
Nb	1	0.00	0.00	0.00	0.07
	6	0.00	0.14	0.13	0.19
	36	0.01	0.01	0.01	0.00
	5	0.00	0.38	0.18	0.28
Mo	1	0.00	0.00	0.03	0.04
	6	0.00	0.35	0.13	0.28
	36	0.19	0.27	0.12	0.15
	17	0.22	0.46	0.18	0.45
Ta	1	0.00	0.00	0.01	0.09
	6	0.00	0.16	0.12	0.24
	36	0.03	0.06	0.06	0.02
	26	0.31	0.072	0.162	0.26
V	1	0.00	0.00	0.15	0.04
	6	0.00	0.15	0.12	0.17
	36	0.02	0.02	0.00	0.01
	27	0.33	0.09	0.16	0.19
W	1	0.24	0.31	0.07	0.43
	6	0.00	0,35	0.10	0.34
	36	0.26	0.26	0.10	0.22
	23	0.279	0.41	0.142	0.52

Appendix E. The difference in PES between the relaxed surface (the system with 2 bottom layers and one metal atom on the surface fixed) and the fixed surface system, the values are in (eV). The values above 0.2 eV is highlighted with grey color.

Sites of H on Metal surface	V	Nb	Ta	Mo	W	Fe	Rh	Ir	Ni	Pd	Pt	Cu	Ag	Au
1	0.04	0.07	0.09	0.04	0.43	0.00	0.00	0.01	0.00	0.00	0.03	0.01	0.01	0.04
2	0.04	0.06	0.09	0.27	0.39	0.00	0.00	0.01	0.01	0.00	0.03	0.03	0.02	0.04
3	0.09	0.09	0.08	0.21	0.31	0.02	0.00	0.01	0.03	0.01	0.02	0.17	0.17	0.05
4	0.25	0.28	0.14	0.49	0.18	0.10	0.01	0.01	0.10	0.10	0.01	0.20	0.19	0.15
5	0.25	0.28	0.26	0.43	0.47	0.12	0.02	0.01	0.07	0.09	0.04	0.12	0.11	0.13
6	0.17	0.19	0.24	0.28	0.34	0.06	0.00	0.01	0.01	0.00	0.01	0.01	0.01	0.03
7	0.04	0.06	0.09	0.27	0.39	0.00	0.00	0.01	0.01	0.00	0.03	0.03	0.02	0.04
8	0.04	0.06	0.08	0.26	0.35	0.00	0.00	0.01	0.01	0.00	0.03	0.05	0.03	0.04
9	0.08	0.07	0.08	0.29	0.34	0.01	0.00	0.01	0.03	0.01	0.02	0.17	0.17	0.05
10	0.23	0.26	0.13	0.48	0.47	0.09	0.01	0.01	0.10	0.09	0.01	0.20	0.18	0.14
11	0.23	0.28	0.26	0.45	0.50	0.12	0.02	0.01	0.07	0.09	0.04	0.12	0.11	0.12
12	0.16	0.19	0.24	0.31	0.38	0.05	0.00	0.01	0.01	0.00	0.01	0.01	0.01	0.03
13	0.10	0.09	0.08	0.21	0.31	0.02	0.00	0.01	0.03	0.01	0.02	0.17	0.17	0.05
14	0.08	0.06	0.08	0.29	0.34	0.01	0.00	0.01	0.03	0.01	0.02	0.17	0.17	0.05
15	0.06	0.05	0.07	0.41	0.45	0.01	0.00	0.01	0.05	0.02	0.02	0.21	0.20	0.04
16	0.18	0.20	0.10	0.43	0.45	0.06	0.00	0.01	0.09	0.08	0.01	0.20	0.17	0.10
17	0.19	0.24	0.23	0.45	0.53	0.09	0.02	0.01	0.07	0.08	0.03	0.11	0.09	0.10
18	0.10	0.14	0.21	0.33	0.44	0.03	0.00	0.01	0.01	0.00	0.02	0.01	0.01	0.03
19	0.25	0.28	0.14	0.49	0.18	0.10	0.01	0.01	0.10	0.10	0.01	0.20	0.19	0.15
20	0.23	0.26	0.13	0.48	0.47	0.09	0.01	0.01	0.10	0.09	0.01	0.20	0.18	0.14
21	0.18	0.20	0.10	0.43	0.45	0.06	0.00	0.01	0.09	0.08	0.01	0.20	0.17	0.10
22	0.33	0.30	0.06	0.36	0.42	0.12	0.00	0.01	0.11	0.09	0.01	0.19	0.16	0.05
23	0.24	0.23	0.05	0.38	0.52	0.13	0.01	0.01	0.06	0.06	0.02	0.10	0.07	0.06
24	0.07	0.05	-0.10	0.27	0.46	0.04	0.00	0.01	0.00	0.00	0.02	0.01	0.00	0.12
25	0.25	0.28	0.26	0.43	0.47	0.12	0.02	0.01	0.08	0.09	0.04	0.12	0.11	0.13
26	0.23	0.28	0.26	0.45	0.50	0.12	0.02	0.01	0.07	0.09	0.04	0.12	0.11	0.12
27	0.19	0.24	0.23	0.45	0.53	0.09	0.02	0.01	0.07	0.08	0.03	0.11	0.09	0.10
28	0.24	0.23	0.05	0.38	0.52	0.13	0.01	0.01	0.06	0.06	0.02	0.10	0.07	0.06
29	0.07	0.05	0.07	0.16	0.30	0.05	0.01	0.01	0.04	0.03	0.01	0.06	0.04	0.02
30	0.02	0.01	0.04	0.14	0.38	0.01	0.00	0.01	0.01	0.00	0.03	0.02	0.00	0.04
31	0.17	0.19	0.24	0.28	0.34	0.06	0.00	0.01	0.01	0.00	0.01	0.01	0.01	0.03
32	0.16	0.19	0.24	0.31	0.38	0.05	0.00	0.01	0.01	0.00	0.01	0.01	0.01	0.03
33	0.10	0.14	0.21	0.33	0.44	0.03	0.00	0.01	0.01	0.00	0.02	0.01	0.01	0.03
34	0.07	0.05	0.10	0.27	0.46	0.04	0.00	0.01	0.00	0.00	0.02	0.01	0.00	0.03
35	0.02	0.01	0.04	0.14	0.38	0.01	0.00	0.01	0.01	0.00	0.03	0.02	0.00	0.04
36	0.01	0.00	0.02	0.15	0.22	0.01	0.00	0.01	0.00	0.00	0.01	0.01	0.00	0.02

Appendix F. Correlation between translation of the surface atoms and energy